ACS Photonics

Article

Cite This: ACS Photonics XXXX, XXX, XXX-XXX pubs.acs.org/journal/apchd5

Electronic Light−Matter Strong Coupling in Nanofluidic Fabry−Pérot Cavities

Hadi Bahsoun,[†] Thibault Chervy,[†] Anoop Thomas,[†] Karl Börjesson,[‡] Manuel Hertzog,[†] Jino George,[†] Eloïse Devaux,[†] Cyriaque Genet,[†] James A. Hutchison,*[,†] and Thomas W. Ebbesen*[,†]

[†]University of Strasbourg, CNRS, ISIS & icFRC, 8 Allée Gaspard Monge, 67000 Strasbourg, France

[‡]Department of Chemistry and Molecular Biology, University of Gothenburg, 41296 Gothenburg, Sweden

Supporting Information

ABSTRACT: Electronic light−matter strong coupling has been limited to solid molecular films due to the challenge of preparing optical cavities with nanoscale dimensions. Here we report a technique to fabricate such Fabry−Pérot nanocavities in which solutions can be introduced such that light−molecule interactions can be studied at will in the liquid phase. We illustrate the versatility of these cavities by studying the emission properties of Chlorin e6 solutions in both the weak and strong coupling regimes as a function of cavity detuning. Liquid nanocavities will broaden the investigation of strong coupling to many solution-based molecular processes.

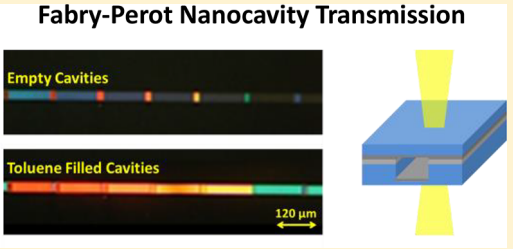

KEYWORDS: *Rabi splitting, Chlorin e6, quantum yield, fluorescence lifetime decay, radiative and nonradiative decay rates*

In the past years, studies have shown that light−matter strong coupling and the associated formation of hybrid light−matter states (Figure 1a) give rise to molecular and material properties that are different than those of the original constituents, i.e., the light mode and the molecule undergoing the coupling. The modified spectra and relaxation processes of organic molecules in the strong coupling (SC) regime have been explored in detail in several experimental configurations[1−17] and studied theoretically by many groups.[18−25] Many processes and properties are modified under strong coupling, such as the rate of nonradiative energy transfer,[26] the conductivity and work function of semiconducting materials,[27,28] the nonlinear response,[29−31] and the rate of chemical reactions.[32,33] These works have been explored in the solid state, even though the photonic nanostructure/molecular film may be suspended in liquid[34,35] or interact with a gas phase.[36]

In the presence of this growing interest in studying strongly coupled materials, there is a need to explore SC of molecules in liquid solutions since that it is the natural condition of many molecular processes. Experiments in liquid solutions have only been achieved for vibrational strong coupling (VSC), which is facilitated by the fact that the vibrational modes are in the IR, which allows one to use microfluidic Fabry−Pérot (FP) cavities (e.g., spacing 1−10 μm).[15,32,37−42] In contrast, electronic strong coupling (ESC) of molecules in the liquid form has not been reported yet for the simple reason that the cavity length in the visible is on the order of 100 nm, which is technically very challenging. Among other things, the nanofluidic FP cavity mirrors (Figure 1b) need to be uniformly flat on a scale much smaller than the cavity length and the cavity must be accessible to the solution.

Here we report the fabrication of nanofluidic FP cavities tunable over a wide range of visible wavelengths that can be filled with liquids. To illustrate the potential of such cavities, we study the photophysical properties of a chlorophyll analogue, Chlorin e6 (Ce6), shown in Figure 1c, in both the weak and strong coupling regimes. In particular, we compare the emission quantum yield and the radiative rate constant as a function of detuning in both regimes, which highlights the distinct features of the strong coupling condition.

We recall that when a material with a well-defined transition dipole moment is placed in an electromagnetic (EM) environment with eigenmodes, such as a FP cavity, that are resonant with the material's transition energy, they may interact by exchanging energy through successive absorption−emission events. If the energy exchange rate is faster than any dissipation in the system, the interaction will give rise to two new light−matter hybrid or polaritonic states, and the system is said to be in the strong coupling regime.[43] The two new states, P^+ and P^-, shown in Figure 1a, are separated by an energy called the Rabi splitting ($\hbar\Omega_R$), which is directly proportional to the scalar product of the electric field $\vec{E}$ of the photonic mode and the transition dipole moment $\vec{d}$ of the material and is given by the following equation:

$$\hbar\Omega_R = 2\vec{E}\cdot\vec{d} \times \sqrt{n_{ph} + 1} = 2\sqrt{\frac{\hbar\omega}{2\varepsilon_0 V}}\, d\sqrt{n_{ph} + 1} \quad (1)$$

Special Issue: Strong Coupling of Molecules to Cavities

Received: June 26, 2017
Published: October 11, 2017

© XXXX American Chemical Society

DOI: 10.1021/acsphotonics.7b00679
ACS Photonics XXXX, XXX, XXX−XXX

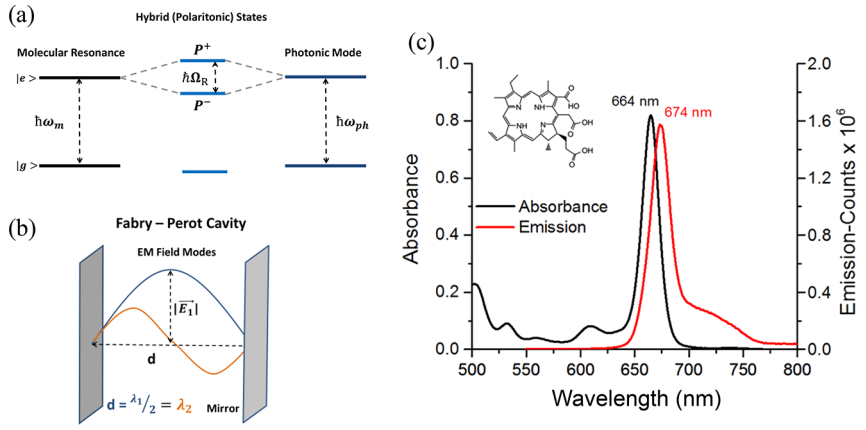

Figure 1. (a) Schematic representation of the coupling of a molecular transition of energy $\hbar\omega_m$ and an optical resonance of energy $\hbar\omega_{ph}$ forming the hybrid states P^+ and P^- separated by the Rabi splitting energy $\hbar\Omega_R$. (b) Schematic illustration of the amplitude of the first and second Fabry–Pérot (FP) cavity modes confined between two metallic mirrors. (c) Absorbance and emission spectra of Chlorin e6 solution in DMF (4.5×10^{-5} M) and its molecular structure.

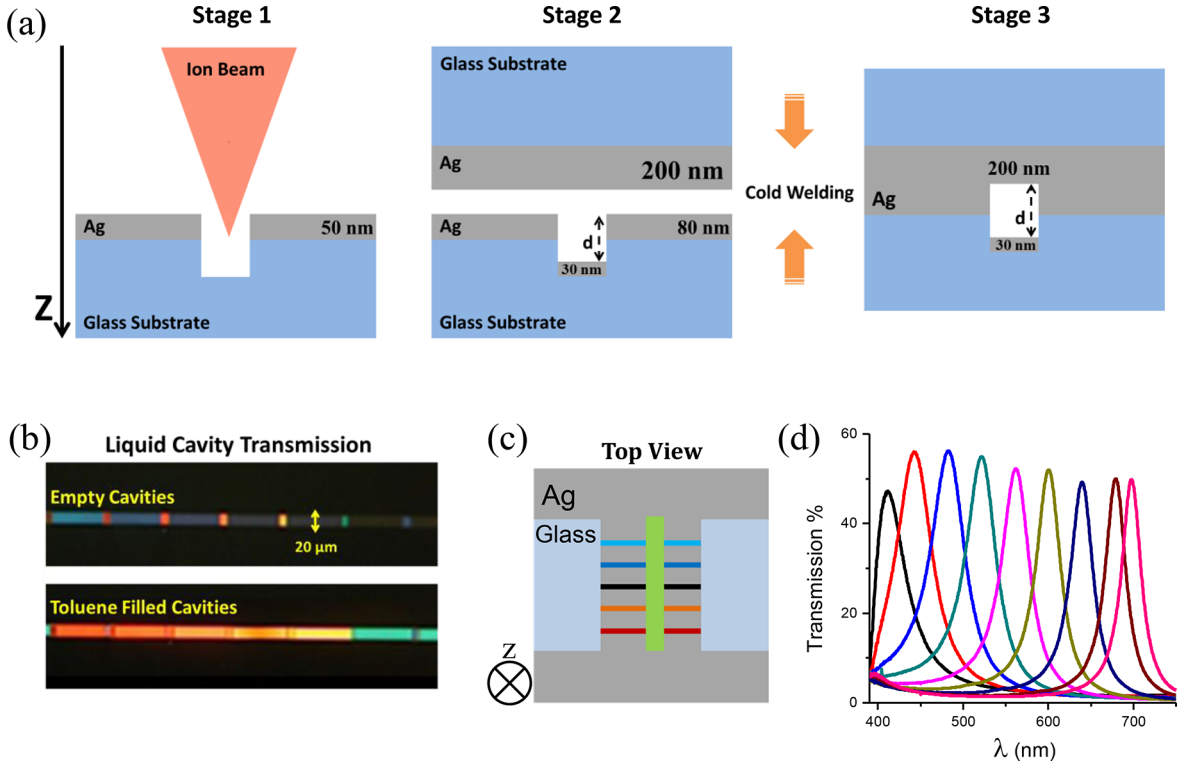

Figure 2. (a) Fabrication stages of nanocavities of thickness d, starting by milling through the Ag layer and glass substrate (stage 1), then Ag evaporation on the milled channels (stage 2), and finally cold-welding both substrates under high pressure (stage 3). (b) Optical micrographs showing white light transmission through the nanofluidic FP cavities before and after filling them with toluene. The colored rectangles represent FP cavities of varying thickness along one single channel, with the corresponding wavelength shift of the confined light mode. (c) Schematic representation of the top view of samples used for our emission experiments in which long channels of a single thickness were milled in a parallel configuration. Each cavity is represented by a colored line based on its optical mode energy detuning relative to the molecule's absorption transition at 664 nm (*i.e.*, cavities with photonic modes in neat DMF at 567 nm (light blue), 631 nm (blue), 665 nm (black), 678 nm (orange), and 733 nm (red)). The areas with neither top nor bottom mirror that act as reservoirs for liquid to enter the cavity are labeled "glass". The green horizontal rectangle is an area with only one mirror. (d) Transmission spectra through empty nanocavities, showing the photonic mode resonance as a function of cavity path length between 200 and 350 nm fabricated by varying the number of FIB milling repeats.

where ε_0 is the permittivity of free space, V is the volume of the confined mode, and n_{ph} is the number of photons in the system. It can be seen from eq 1 that when the number of photons in the system goes to zero, the Rabi splitting still has a finite value. This is due to the interaction of the material with the zero-point energy fluctuations of the confined mode. In this case, the system is in the vacuum Rabi regime, the conditions of all our experiments in this work. For a system with N molecules coupled to a resonant mode, the Rabi splitting is directly proportional to the square root of the concentration of molecules coupled to the field since $\hbar\Omega_R \propto \sqrt{N/V} = \sqrt{C}$. So as we will show later, decreasing the concentration is one way

DOI: 10.1021/acsphotonics.7b00679
ACS Photonics XXXX, XXX, XXX−XXX

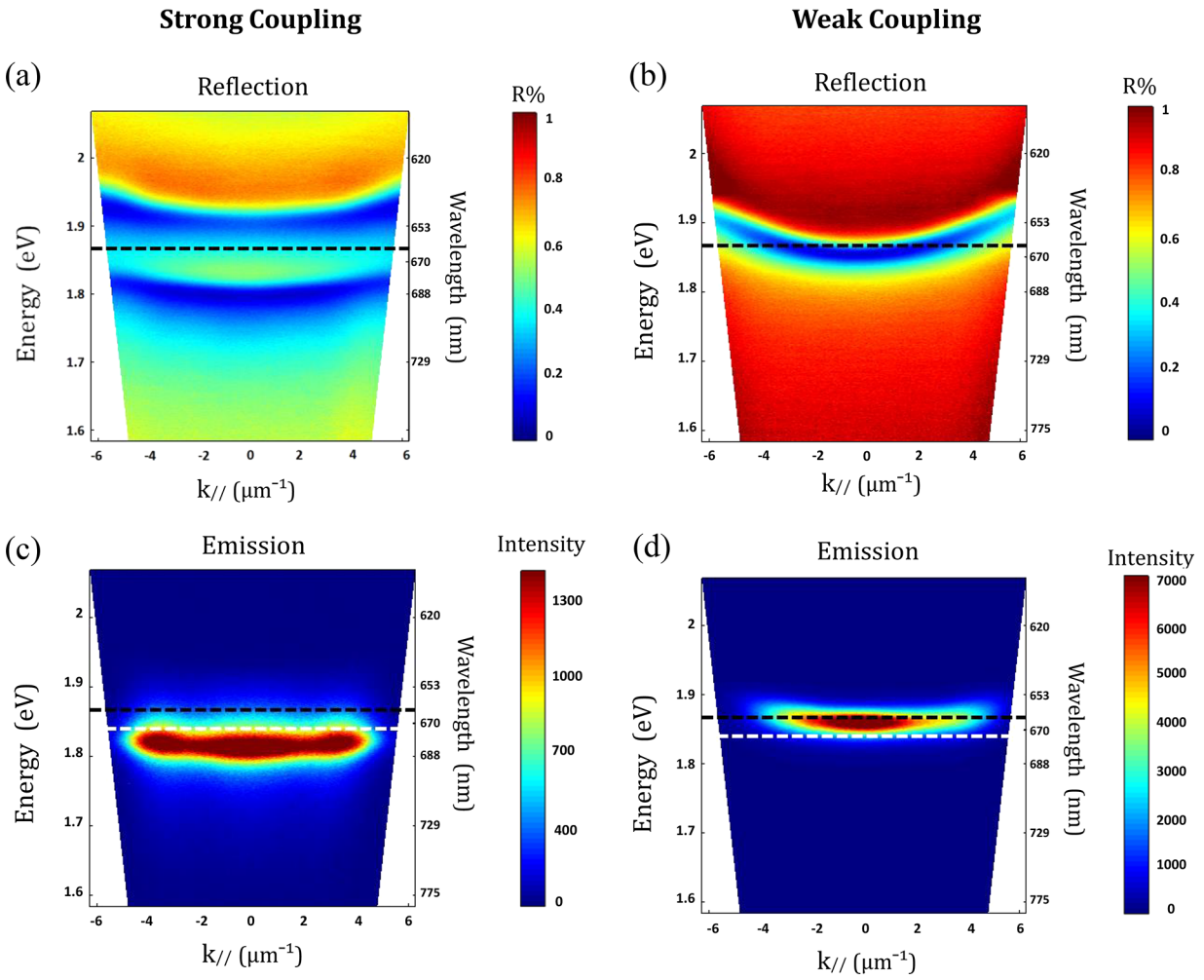

Figure 3. Angle-resolved dispersion reflection spectra from high concentration (strong coupling regime) (a) and low concentration (weak coupling regime) (b) Ce6/DMF solution-filled cavities resonant with the Ce6 transition energy (black dashed lines). The emission dispersion curves from the same cavities are shown in (c) and (d) with normal incidence excitation at 532 nm. The white dashed line in (c) and (d) represents the emission from uncoupled molecules. Note that the dispersion of the emission could only be collected over a limited angle due to the sidewalls of the cavities; this is visible in (c) at high $k_{\|}$ values.

to bring the system from the strong to the weak coupling regime.

Chlorin e6 has a sharp absorption peak (Q-band) at 664 nm and fluoresces with a small Stokes shift at 674 nm (Figure 1c). In addition to these spectral features, which are very suitable for studying light−matter interactions, it is characterized by high solubility in many solvents without forming aggregates.[44] In dilute conditions, it has a reasonably long fluorescence lifetime (4.4 ns) and a good emission quantum yield (~15% in ethanol).[45,46] These characteristics make Ce6 a good candidate among organic molecules for exploring liquid phase photoemission and relaxation processes under both strong and weak coupling regimes.

To prepare the nanofluidic FP cavity having two parallel metallic mirrors separated by a distance d on the order of 100 nm, we developed the following technique (see Supporting Information for full details). The sample preparation starts by evaporating a 50 nm thick Ag layer on a 2.5 cm × 2.5 cm glass substrate. The sample is then introduced in a Zeiss Auriga focused ion beam (FIB) apparatus, and a ca. 10−20 μm × 120 μm rectangular area is milled through the Ag layer and into the glass substrate to create the nanofluidic channel (Figure 2a). After the milling, another 30 nm of Ag is evaporated on the substrate to act as the cavity's bottom mirror. Another identical glass substrate with a Ag layer acting as the cavity's top mirror is also prepared. Then the two substrates are cold-welded by high pressure (~1.6 tons/cm^2) using a press normally employed for preparing pellets for IR measurements (Figure 2a). Cold-welding has already been used successfully to make solid state cavities.[47,48] A first set of cavities with increasing depth were milled along a line in the middle of the sample, connected between each other by a very small overlap area resulting in a few millimeters long channel as shown in Figure 2b with and without solvent. The thickness of the top mirror layer depends on the required measurements. For instance, we used a 30 nm top Ag mirror when probing the cavities in transmission mode (as illustrated in Figure 2b) and 200 nm when characterizing the spectra in reflection mode. It is important to note that a 2 nm Cr film layer is always present between the glass substrate and the Ag film in order to ensure strong adhesion.

Finally, to introduce the molecules into the nanofluidic channels, the sample is simply dipped into the liquid solution, which is drawn in by capillary force. We have verified that many solvents including water wet the channels and therefore are spontaneously pulled in. However, we found that the drawing up of liquid was easiest in nanofluidic FP cavities of single

DOI: 10.1021/acsphotonics.7b00679
ACS Photonics XXXX, XXX, XXX−XXX

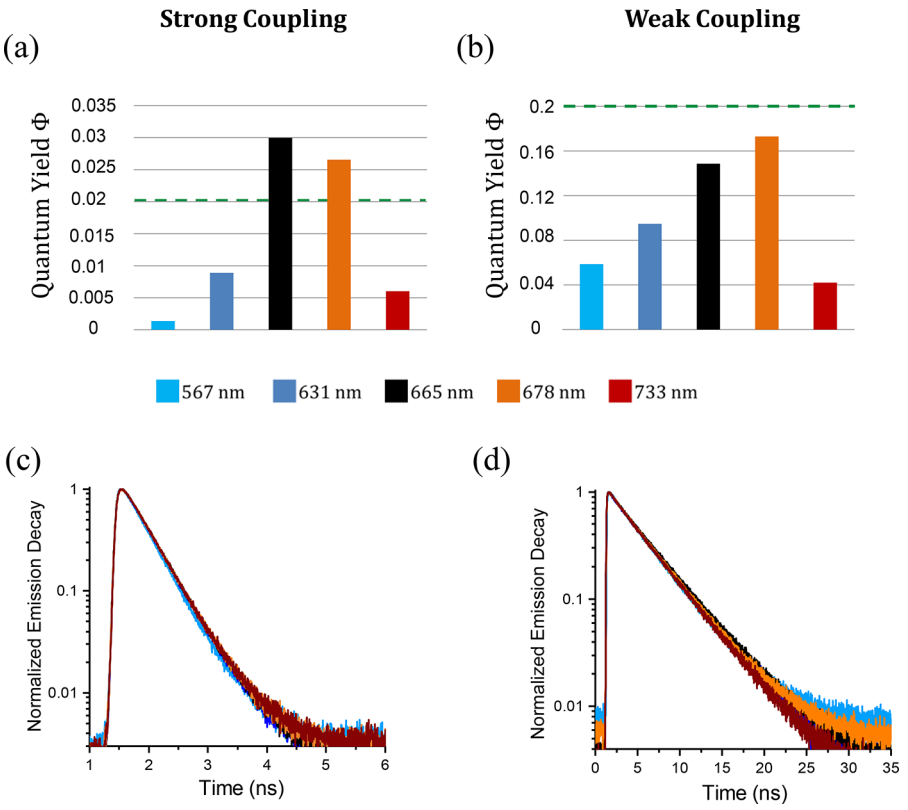

Figure 4. (a and b) Emission quantum yields (±10%) as a function of cavity mode detuning in the strong and weak coupling regimes, respectively, for Ce6 in DMF solution; (c and d) corresponding decays for the same cavities as in (a) and (b), respectively. Each cavity is represented by a colored cylinder based on its optical mode energy detuning relative to the molecule's absorption transition at 664 nm (i.e., cavities with photonic modes in neat DMF at 567 nm (light blue), 631 nm (blue), 665 nm (black), 678 nm (orange), and 733 nm (red)). The resonant case is in black. The green lines in (a) and (b) correspond to the emission quantum yields of the bare molecule at the same concentrations.

optical path length, and so we prepared cavities with different resonances in parallel as illustrated in Figure 2c for the experiments in this work. Here areas at both ends of the cavity channels were masked during metal evaporation to form a metal-free space acting as a reservoir for the liquid to fill the channels. In addition, a mask was placed over parts of the milled channels (illustrated by the green rectangle in Figure 2c) before evaporating the bottom mirror to create in each channel one-sided mirror areas in order to provide a noncavity reference for the same solution.

The thickness of the nanofluidic FP cavity was controlled by milling different depths in the bottom substrate. High control over the cavity mode resonance is achieved by programming a large number of repeats on the Zeiss Auriga FIB to mill a given thickness. This enables very flat surfaces (less than a few nm variations over 5 μm) on which the mirror can then be deposited (see SI). In Figure 2d, the transmission resonance of various channels is shown as a function of ion beam milling repeats. Under our milling conditions, the peak position moves by ca. 20 nm for every 1000 repeats, reflecting the change in FP path length d, as also can be seen in the colors of Figure 2b. The color changes again upon introduction of a solvent (here toluene) due to the increased medium refractive index inside the channel. The Q-factor of such cavities ranges between 20 and 60, depending on the type of metal (e.g., the imaginary part of the dielectric constant) and the mode used. In this regard, we were also able to reproduce similar cavities with Au mirrors. It should be noted that the choice of metal depends on the wavelength of interest; for example, Ag yields a smaller fwhm than Au in the visible due to the smaller value of the imaginary part ε'' of its dielectric constant. The ability to mill FP nanocavities of 100s of micrometers lateral extent with a desired shape, in different metals, and with very high control of cavity thickness, is an outstanding point of our fabrication method, making these nanofluidic structures ideal for studying molecules in solutions in the weak and strong coupling regimes.

To study the properties of Ce6 under weak and strong coupling regimes in liquid solution, samples with parallel FP cavities, such as in Figure 2c, were prepared with a thick top mirror so that the spectroscopic measurements could be recorded in reflection mode. This has no particular consequence on the Q-factor.

Solutions of Ce6 in dimethylformamide (DMF) at high (0.18 M) and low concentrations (3.6 mM) were introduced into the nanocavities by capillarity. In Figure 3a and b respectively are shown reflection dispersion spectra for FP cavities with Ce6 solutions at two concentrations corresponding to the weak and strong coupling regime, respectively. The cavities are thickness-tuned such that their λ mode (Figure 1b) sweeps through the Ce6 absorption peak at 664 nm as a function of angle of interrogation. In Figure 3a, a mode splitting can be seen due to the strength of the interaction between the mode and molecular transition (represented by the dashed line in Figure 3b). The splitting has a value of ca. 110 meV, which is larger than the full width at half-maximum (fwhm) of both the molecular absorption peak (67 meV) and the FP resonance (62 meV). The system is therefore clearly in the strong coupling regime. The polaritonic states are dispersive due to the photonic

DOI: 10.1021/acsphotonics.7b00679
ACS Photonics XXXX, XXX, XXX−XXX

character they inherit from the FP mode. As discussed in the introduction, the Rabi splitting depends on the square root of the Ce6 concentration (see Figure S2 in the SI), and at a certain threshold when the Rabi splitting becomes smaller than the fwhm of the original components, the system is no longer in the strong coupling regime. This is the case when the concentration is decreased by a factor of ca. 50, such as in Figure 3b. The FP mode then displays the normal parabolic dispersive shape and the system is in the weak coupling regime with no avoided crossing at the molecular absorption.

The emission dispersions in the strong and weak coupling regimes at resonance are displayed in Figure 3c and d. The emission of P^- in the strong coupling case (Figure 3c) is at slightly lower energies than the Ce6 emission in the weak coupling regime, and only the reflection dispersion curves reveal unambiguously whether the system is in the weak or strong coupling regimes. For ease of comparison, black and white dashed lines were added in Figure 3c and d and correspond respectively to the absorption and emission maxima of the bare molecule. As can be seen, in the weak coupling limit, the emission is out-coupled through the cavity mode where the local density of optical states is highest. As we will see next, the effects of the coupling regime on the emission quantum yield and radiative lifetimes are quite distinct.

The emission quantum yield Φ values were determined relative to that of dilute solutions of the bare Ce6, using the following equation:[49]

$$\Phi_c = \Phi_R \frac{A_R(\lambda_{ex})}{E_R} \frac{E_c}{A_c(\lambda_{ex})} \frac{n_c^2(\lambda_{em})}{n_R^2(\lambda_{em})} \quad (2)$$

where A is the fractional absorption $(1-10^{-\text{Absorbance}})$ at the excitation wavelength, E the integral of emission counts, and n the index of refraction of the solvent at the emission wavelength. Indices c and R represent the cavity and the reference molecule (Ce6), respectively. The quantum yield values for cavity emission were obtained through a procedure that is explained in detail in the SI. Importantly, the quantum yields were referenced to Ce6 in dilute ethanol,[45,46] and transfer matrix simulations were used to determine the absorption in the Ce6/DMF layer in each cavity. Note that at high concentration, excimer emission is apparent at long wavelengths, >740 nm, for highly concentrated solutions, and we excluded this from the analysis as explained in the Experimental Methods section. Reabsorption of the emission is minimal (<0.5%) even at the highest concentration used for strong coupling due to the extremely short path length.

Figure 4a and b show the variation of the emission quantum yield as a function of cavity mode detuning in the strong and weak coupling regimes, respectively. While the absolute values of Φ are determined within ±10%, the relative values between different detunings are accurate up to the signal-to-noise ratio of the spectroscopic equipment. First, we observe that the emission quantum yields in the strong coupling case are always much lower than those in the weak coupling case due to self-quenching at high Ce6 concentration, discussed further down. In the strong coupling regime, the maximal quantum yield is achieved for the resonant cavity and decreases when the cavity is blue or red detuned. The yield at resonance is much higher than that of the bare molecule at the same concentration (dashed line in Figure 4a). This likely reflects the enhanced radiative nature of the collective polaritonic state, and indeed the radiative rate constant k_r (extracted from the emission lifetimes (τ) (Figures 4c,d) and the quantum yield as $k_r = \Phi/\tau$) follows the same trend as the quantum yield for different detunings (see Table 1). Other studies have found both enhanced and suppressed emission quantum yields under strong coupling.[4,5,10] Such variations, which depend on the coupled molecules and the experimental conditions, reflect most likely differences in the nonradiative channels available for decay and the fact that Φ is dominated by k_{nr}[4,5,10] (e.g., values in Table 1).

Table 1. Measured Fluorescence Quantum Yield (Φ), Fluorescence Lifetime (τ), and Calculated Radiative Rate Constant (k_r) and Nonradiative Rate Constant (k_{nr}) for DMF Solutions of Chlorin e6 of 0.18 M Concentration (Strong Coupling Regime) and 3.6 mM Concentration (Weak Coupling Regime) in Fabry–Pérot Nanocavities with Optical Modes of Various Detunings (the on-Resonance Mode is Highlighted in Italics) Relative to the Chlorin e6 Absorption at 664 nm

	Strong Coupling			
cavity resonance	Φ	τ (ns)	k_r (s^{-1})	k_{nr} (s^{-1})
567 nm	1.4×10^{-3}	0.40	3.4×10^{6}	2.5×10^{9}
631 nm	8.9×10^{-3}	0.42	2.1×10^{7}	2.4×10^{9}
665 nm	*3.0×10^{-2}*	*0.42*	*7.1×10^{7}*	*2.3×10^{9}*
678 nm	2.7×10^{-2}	0.42	6.3×10^{7}	2.3×10^{9}
733 nm	6.0×10^{-03}	0.43	1.4×10^{7}	2.3×10^{9}
	Weak Coupling			
cavity resonance	Φ	τ (ns)	k_r (s^{-1})	k_{nr} (s^{-1})
567 nm	5.9×10^{-2}	4.0	1.5×10^{7}	2.3×10^{8}
631 nm	9.5×10^{-2}	4.4	2.2×10^{7}	2.1×10^{8}
665 nm	*1.5×10^{-1}*	*4.5*	*3.3×10^{7}*	*1.9×10^{8}*
678 nm	1.7×10^{-1}	4.2	4.1×10^{7}	2.0×10^{8}
733 nm	4.2×10^{-2}	4.2	1.0×10^{7}	2.3×10^{8}

However, a different trend was observed in the weak coupling case; here the emission quantum yield is maximum when the cavity mode overlaps with the Ce6 fluorescence (orange bar in Figure 4b). Again this correlates with the extracted radiative rate (Table 1) and is the trend one would expect from a Purcell effect on the radiative decay rate of the molecule. It should however be noted that the emission quantum yield does not exceed that of the bare molecule in solution, perhaps because we are observing an averaging effect across the mode amplitude, with some molecules experiencing very high mode density but others being at the central node or near the mirrors (Figure 1b). Additionally, subpopulations of molecules within a few nanometers of the metal mirrors might be quenched, influencing the average result.

In contrast to the quantum yields, the emission lifetimes measured from the cavities are nearly invariant as a function of detuning in both the weak and strong coupling regime. This is because the nonradiative rate constant k_{nr} dominates k_r in both weak and strong coupling regimes (Table 1). In the weak coupling limit (3.6 mM Ce6), k_{nr} is determined mainly by the internal vibrational relaxation and intersystem crossing, as its lifetime of ∼4.3 ns is similar to that in 10^{-5} M solutions, where interactions between Ce6 molecules within the excited state lifetime are unlikely. In the strong coupling limit (0.18 M Ce6), excited Ce6 can also be quenched efficiently by interaction with surrounding Ce6 molecules in the ground state (self-quenching), increasing k_{nr} by an order of magnitude. For

DOI: 10.1021/acsphotonics.7b00679
ACS Photonics XXXX, XXX, XXX–XXX

instance, if we assume a diffusion-limited rate constant for the encounter between an excited Ce6 and a ground state Ce6, e.g., 10^{10} M^{-1} s^{-1}, and multiply it by the concentration of Ce6 in the strong coupling case (0.18 M), the rate is 1.8×10^9 s^{-1}, a value very close to the k_{nr} under strong coupling of ca. 2.3×10^9 s^{-1} (Table 1).

In summary, we have succeeded in preparing nanoscale liquid Fabry–Pérot nanocavities that have the excellent optical qualities necessary to observe strong coupling effects for molecular solutions. In particular we demonstrate the enhanced radiative nature of polaritonic states generated from concentrated DMF solutions of Chlorin e6. Our fabrication method allows for the facile preparation of FP nanocavities of any desired lateral shape and lateral extent up to the millimeter scale, but with exquisite control over the nanoscale thickness. Thus, samples can be customized to various geometries and length scales for different experimental purposes. While these FP nanocavities were made with Ag mirrors, we have tested that the same approach can be used for other metals such as Au. Furthermore, many solvents including water are easily taken up by our cavities such that studies of biological systems in their native solvation environment become possible. The observation of light–matter strong coupling of electronic transitions in the liquid state opens the possibility to study other molecular processes in this regime where diffusion and orientation play a role, such as chemistry, with potential to broaden the scope of this field immensely.

EXPERIMENTAL METHODS

Reflection Dispersion Measurements. A home-built microscopy setup was used for the dispersive reflection and emission spectra. It consists of a microscope lens that focuses a broad band white light source (DH-2000-BAL, Ocean Optics) onto the cavity of interest. The reflected light was imaged on the slit of a monochromator (Princeton Instruments), couple to a charge-coupled device (CCD, Pixis, Princeton Instruments) detector to register the spectra. By using a Fourier lens with an F-number of 0.5 (5 cm diameter, 10 cm focal length), the angle-resolved reflection spectra could be obtained. The reflection dispersion spectra were acquired for each cavity thickness, for solutions of both high concentration (strong coupling regime) and low concentration (weak coupling regime). The same microscopy setup was used to obtain the angle-resolved emission from each cavity. The system was excited at 532 nm using a continuous wave diode laser (Oxxius) with a focal spot of ~1.2 μm diameter and ~160 μW power. It should be noted that the emission properties are independent of excitation wavelength.

Emission Spectra Measurements at Normal Incidence. The emission spectra of the samples were collected in reflection mode using a Nikon Eclipse TE200 light microscope, with a Nikon 40× objective having a 0.6 numerical aperture (NA) and 3.7–2.7 mm working distance (WD). After focusing at a point in the filled cavity, the system was excited in *epi* configuration by UV light produced by a mercury short arc HBO lamp (OSRAM). The excitation light was filtered by a Semrock bandpass filter centered at 365 nm. The emitted light from the cavities was collected by a spectrograph/CCD camera (Acton SP-300i/Roper ST133) coupled to the microscope. The emission spectrum was also recorded from the same channels in a region with only one mirror, the latter representing emission from the bare molecules. Emission spectra recorded for different cavity thicknesses recorded at normal incidence are shown in Figure S3. As can be seen in Figure S3a, when the cavity is strongly red-detuned, a large emission peak appears. This is especially apparent at high concentrations of Ce6 (0.18 M) used to achieve strong coupling and is attributed to excimer emission, peaking outside the cavity at ca. 745 nm (inset, Figure S3a). The fluorescence lifetime of the emission at 740 nm is longer than that observed for monomeric Ce6, while the excitation spectrum of this emission matches that of monomeric Ce6, perfectly in keeping with the emission properties of an excimer. This red-shifted emission of >740 nm was thus excluded from the quantum yield determinations.

Lifetime Measurements. The emission lifetimes were measured using the time-correlated single photon counting technique on a Nikon Eclipse Ti confocal microscope coupled to a PicoQuant PicoHarp 300 pulse correlator. A 40× objective with 0.6 NA and 3.7–2.7 WD was employed. The excitation source was a picosecond pulsed diode laser (PicoQuant PDL 800-D) at 640 nm, with an instrument response-limited pulse width of 83 ps, repetition rate of 80 MHz, and average power of 9 mW. The emitted photons were detected by a single-photon avalanche diode detector. A 685 ± 10 nm bandpass filter was placed before the detector in order to measure emission only from monomeric Ce6–cavity interactions. The emission decay lifetimes could be well fit by single-exponential decay profiles in all cases using PicoQuant SymphoTime64 software.

ASSOCIATED CONTENT

Supporting Information

The Supporting Information is available free of charge on the ACS Publications website at DOI: 10.1021/acsphotonics.7b00679.

Sample and solution preparation; SEM top view for the milled channel; AFM for surface roughness; Rabi splitting as a function of molecular concentration; emission spectra from cavities with different detuning; quantum yield detailed calculation procedure (PDF)

AUTHOR INFORMATION

Corresponding Authors

*E-mail: ebbesen@unistra.fr.
*E-mail: hutchison@unistra.fr.

ORCID

Thomas W. Ebbesen: 0000-0002-3999-1636

Notes

The authors declare no competing financial interest.

ACKNOWLEDGMENTS

We acknowledge support of the International Center for Frontier Research in Chemistry (icFRC, Strasbourg), the ANR Equipex Union (ANR-10-EQPX-52-01), the Labex NIE projects (ANR-11-LABX-0058 NIE), and CSC (ANR-10-LABX- 0026 CSC) within the Investissement d'Avenir program ANR-10-IDEX-0002-02.

REFERENCES

(1) Törmä, P.; Barnes, W. L. Strong Coupling between Surface Plasmon Polaritons and Emitters: A Review. *Rep. Prog. Phys.* **2015**, *78*, 13901.

(2) Ebbesen, T. W. Hybrid Light–Matter States in a Molecular and Material Science Perspective. *Acc. Chem. Res.* **2016**, *49*, 2403–2412.

DOI: 10.1021/acsphotonics.7b00679
ACS Photonics XXXX, XXX, XXX–XXX

(3) Bellessa, J.; Symonds, C.; Laverdant, J.; Benoit, J.-M.; Plenet, J. C.; Vignoli, S. Strong Coupling between Plasmons and Organic Semiconductors. *Electronics* **2014**, *3*, 303−313.
(4) Ballarini, D.; De Giorgi, M.; Gambino, S.; Lerario, G.; Mazzeo, M.; Genco, A.; Accorsi, G.; Giansante, C.; Colella, S.; D'Agostino, S.; Cazzato, P.; Sanvitto, D.; Gigli, G. Polariton-Induced Enhanced Emission from an Organic Dye under the Strong Coupling Regime. *Adv. Opt. Mater.* **2014**, *2*, 1076−1081.
(5) Wang, S.; Chervy, T.; George, J.; Hutchison, J. A.; Genet, C.; Ebbesen, T. W. Quantum Yield of Polariton Emission from Hybrid Light-Matter States. *J. Phys. Chem. Lett.* **2014**, *5*, 1433−1439.
(6) Tanyi, E. K.; Thuman, H.; Brown, N.; Koutsares, S.; Podolskiy, V. A.; Noginov, M. A. Control of the Stokes Shift with Strong Coupling. *Adv. Opt. Mater.***2017**, *5*, 160094110.1002/adom.201600941.
(7) Wersäll, M.; Cuadra, J.; Antosiewicz, T. J.; Balci, S.; Shegai, T. Observation of Mode Splitting in Photoluminescence of Individual Plasmonic Nanoparticles Strongly Coupled to Molecular Excitons. *Nano Lett.* **2017**, *17*, 551−558.
(8) Baieva, S.; Hakamaa, O.; Groenhof, G.; Heikkilä, T. T.; Toppari, J. J. Dynamics of Strongly Coupled Modes between Surface Plasmon Polaritons and Photoactive Molecules: The Effect of the Stokes Shift. *ACS Photonics* **2017**, *4*, 28−37.
(9) Wang, H.; Toma, A.; Wang, H.-Y.; Bozzola, A.; Miele, E.; Haddadpour, A.; Veronis, G.; De Angelis, F.; Wang, L.; Chen, Q.-D.; Xu, H.-L.; Sun, H.-B.; Zaccaria, R. P. The Role of Rabi Splitting Tuning in the Dynamics of Strongly Coupled J-Aggregates and Surface Plasmon Polaritons in Nanohole Arrays. *Nanoscale* **2016**, *8*, 13445−13453.
(10) Grant, R. T.; Michetti, P.; Musser, A. J.; Gregoire, P.; Virgili, T.; Vella, E.; Cavazzini, M.; Georgiou, K.; Galeotti, F.; Clark, C.; Clark, J.; Silva, C.; Lidzey, D. G. Efficient Radiative Pumping of Polaritons in a Strongly Coupled Microcavity by a Fluorescent Molecular Dye. *Adv. Opt. Mater.* **2016**, *4*, 1615−1623.
(11) Zengin, G.; Johansson, G.; Johansson, P.; Antosiewicz, T. J.; Käll, M.; Shegai, T. Approaching the Strong Coupling Limit in Single Plasmonic Nanorods Interacting with J-Aggregates. *Sci. Rep.* **2013**, *3*, 3074.
(12) Shalabney, A.; George, J.; Hutchison, J. a.; Pupillo, G.; Genet, C.; Ebbesen, T. W. Coherent Coupling of Molecular Resonators with a Microcavity Mode. *Nat. Commun.* **2015**, *6*, 5981.
(13) Muallem, M.; Palatnik, A.; Nessim, G. D.; Tischler, Y. R. Strong Light-Matter Coupling between a Molecular Vibrational Mode in a PMMA Film and a Low-Loss Mid-IR Microcavity. *Ann. Phys.* **2016**, *528*, 313−320.
(14) Long, J. P.; Simpkins, B. S. Coherent Coupling between a Molecular Vibration and Fabry−Pérot Optical Cavity to Give Hybridized States in the Strong Coupling Limit. *ACS Photonics* **2015**, *2*, 130−136.
(15) Vergauwe, R. M. A.; George, J.; Chervy, T.; Hutchison, J. A.; Shalabney, A.; Torbeev, V. Y.; Ebbesen, T. W. Quantum Strong Coupling with Protein Vibrational Modes. *J. Phys. Chem. Lett.* **2016**, *7*, 4159−4164.
(16) Schwartz, T.; Hutchison, J. A.; Léonard, J.; Genet, C.; Haacke, S.; Ebbesen, T. W. Polariton Dynamics under Strong Light-Molecule Coupling. *ChemPhysChem* **2013**, *14*, 125−131.
(17) Vasa, P.; Pomraenke, R.; Cirmi, G.; De Re, E.; Wang, W.; Schwieger, S.; Leipold, D.; Runge, E.; Cerullo, G.; Lienau, C. Ultrafast Manipulation of Strong Coupling in Metal−Molecular Aggregate Hybrid Nanostructures. *ACS Nano* **2010**, *4*, 7559−7565.
(18) George, J.; Wang, S.; Chervy, T.; Canaguier-Durand, A.; Schaeffer, G.; Lehn, J.-M.; Hutchison, J. a; Genet, C.; Ebbesen, T. W. Ultra-Strong Coupling of Molecular Materials: Spectroscopy and Dynamics. *Faraday Discuss.* **2015**, *178*, 281−294.
(19) Schachenmayer, J.; Genes, C.; Tignone, E.; Pupillo, G. Cavity-Enhanced Transport of Excitons. *Phys. Rev. Lett.* **2015**, *114*, 1−6.
(20) Flick, J.; Ruggenthaler, M.; Appel, H.; Rubio, A. Atoms and Molecules in Cavities, from Weak to Strong Coupling in Quantum-Electrodynamics (QED) Chemistry. *Proc. Natl. Acad. Sci. U. S. A.* **2017**, *114*, 3026−3034.
(21) Herrera, F.; Spano, F. C. Cavity-Controlled Chemistry in Molecular Ensembles. *Phys. Rev. Lett.* **2016**, *116*, 1−6.
(22) Litinskaya, M.; Tignone, E.; Pupillo, G. Cavity Polaritons with Rydberg Blockade and Long-Range Interactions. *J. Phys. B: At., Mol. Opt. Phys.* **2016**, *49*, 164006.
(23) Kowalewski, M.; Bennett, K.; Mukamel, S. Non-Adiabatic Dynamics of Molecules in Optical Cavities. *J. Chem. Phys.* **2016**, *144*, 1−8.
(24) Gentile, M. J.; Horsley, S. A. R.; Barnes, W. L. Localized Exciton−polariton Modes in Dye-Doped Nanospheres: A Quantum Approach. *J. Opt.* **2016**, *18*, 15001.
(25) González-Tudela, A.; Huidobro, P. A.; Martín-Moreno, L.; Tejedor, C.; García-Vidal, F. J. Theory of Strong Coupling between Quantum Emitters and Propagating Surface Plasmons. *Phys. Rev. Lett.* **2013**, *110*, 126801.
(26) Zhong, X.; Chervy, T.; Wang, S.; George, J.; Thomas, A.; Hutchison, J. A.; Devaux, E.; Genet, C.; Ebbesen, T. W. Non-Radiative Energy Transfer Mediated by Hybrid Light-Matter States. *Angew. Chem., Int. Ed.* **2016**, *55*, 6202−6206.
(27) Orgiu, E.; George, J.; Hutchison, J. a.; Devaux, E.; Dayen, J. F.; Doudin, B.; Stellacci, F.; Genet, C.; Schachenmayer, J.; Genes, C.; Pupillo, G.; Samorì, P.; Ebbesen, T. W. Conductivity in Organic Semiconductors Hybridized with the Vacuum Field. *Nat. Mater.* **2014**, *14*, 1123−1130.
(28) Hutchison, J. A.; Liscio, A.; Schwartz, T.; Canaguier-Durand, A.; Genet, C.; Palermo, V.; Samorì, P.; Ebbesen, T. W. Tuning the Work-Function via Strong Coupling. *Adv. Mater.* **2013**, *25*, 2481−2485.
(29) Chervy, T.; Xu, J.; Duan, Y.; Wang, C.; Mager, L.; Frerejean, M.; Münninghoff, J. A. W.; Tinnemans, P.; Hutchison, J. A.; Genet, C.; Rowan, A. E.; Rasing, T.; Ebbesen, T. W. High-Efficiency Second-Harmonic Generation from Hybrid Light-Matter States. *Nano Lett.* **2016**, *16*, 7352−7356.
(30) Plumhof, J. D.; Stöferle, T.; Mai, L.; Scherf, U.; Mahrt, R. F. Room-Temperature Bose−Einstein Condensation of Cavity Exciton−polaritons in a Polymer. *Nat. Mater.* **2013**, *13*, 247−252.
(31) Daskalakis, K. S.; Maier, S. a; Murray, R.; Kéna-Cohen, S. Nonlinear Interactions in an Organic Polariton Condensate. *Nat. Mater.* **2014**, *13*, 271−278.
(32) Thomas, A.; George, J.; Shalabney, A.; Dryzhakov, M.; Varma, S. J.; Moran, J.; Chervy, T.; Zhong, X.; Devaux, E.; Genet, C.; Hutchison, J. A.; Ebbesen, T. W. Ground-State Chemical Reactivity under Vibrational Coupling to the Vacuum Electromagnetic Field. *Angew. Chem., Int. Ed.* **2016**, *55*, 11462−11466.
(33) Hutchison, J. A.; Schwartz, T.; Genet, C.; Devaux, E.; Ebbesen, T. W. Modifying Chemical Landscapes by Coupling to Vacuum Fields. *Angew. Chem., Int. Ed.* **2012**, *51*, 1592−1596.
(34) Ni, W.; Yang, Z.; Chen, H.; Li, L.; Wang, J. Coupling between Molecular and Plasmonic Resonances in Freestanding Dye−Gold Nanorod Hybrid Nanostructures. *J. Am. Chem. Soc.* **2008**, *130*, 6692−6693.
(35) Melnikau, D.; Govyadinov, A. A.; Sánchez-Iglesias, A.; Grzelczak, M.; Liz-Marzán, L. M.; Rakovich, Y. P. Strong Magneto-Optical Response of Nonmagnetic Organic Materials Coupled to Plasmonic Nanostructures. *Nano Lett.* **2017**, *17*, 1808−1813.
(36) Berrier, A.; Cools, R.; Arnold, C.; Offermans, P.; Crego-Calama, M.; Brongersma, S. H.; Gómez-Rivas, J. Active Control of the Strong Coupling Regime between Porphyrin Excitons and Surface Plasmon Polaritons. *ACS Nano* **2011**, *5*, 6226−6232.
(37) George, J.; Chervy, T.; Shalabney, A.; Devaux, E.; Hiura, H.; Genet, C.; Ebbesen, T. W. Multiple Rabi Splittings under Ultrastrong Vibrational Coupling. *Phys. Rev. Lett.* **2016**, *117*, 1−5.
(38) George, J.; Shalabney, A.; Hutchison, J. A.; Genet, C.; Ebbesen, T. W. Liquid-Phase Vibrational Strong Coupling. *J. Phys. Chem. Lett.* **2015**, *6*, 1027−1031.
(39) Casey, S. R.; Sparks, J. R. Vibrational Strong Coupling of Organometallic Complexes. *J. Phys. Chem. C* **2016**, *120*, 28138−28143.
(40) Simpkins, B. S.; Fears, K. P.; Dressick, W. J.; Spann, B. T.; Dunkelberger, A. D.; Owrutsky, J. C. Spanning Strong to Weak Normal Mode Coupling between Vibrational and Fabry−Pérot Cavity

DOI: 10.1021/acsphotonics.7b00679
ACS Photonics XXXX, XXX, XXX−XXX

Modes through Tuning of Vibrational Absorption Strength. *ACS Photonics* **2015**, *2*, 1460−1467.
(41) Dunkelberger, A. D.; Spann, B. T.; Fears, K. P.; Simpkins, B. S.; Owrutsky, J. C. Modified Relaxation Dynamics and Coherent Energy Exchange in Coupled Vibration-Cavity Polaritons. *Nat. Commun.* **2016**, *7*, 13504.
(42) Trichet, A. A. P.; Foster, J.; Omori, N. E.; James, D.; Dolan, P. R.; Hughes, G. M.; Vallance, C.; Smith, J. M. Open-Access Optical Microcavities for Lab-on-a-Chip Refractive Index Sensing. *Lab Chip* **2014**, *14*, 4244−4249.
(43) Haroche, S.; Kleppner, D. Cavity Quantum Electrodynamics. *Phys. Today* **1989**, *42*, 24−30.
(44) Paul, S.; Heng, P. W. S.; Chan, L. W. Optimization in Solvent Selection for Chlorin e6 in Photodynamic Therapy. *J. Fluoresc.* **2013**, *23*, 283−291.
(45) Zenkevich, E.; Sagun, E.; Knyukshto, V.; Shulga, A.; Mironov, A.; Efremova, O.; Bonnett, R.; Songca, S. P.; Kassem, M. Photophysical and Photochemical Properties of Potential Porphyrin and Chlorin Photosensitizers for PDT. *J. Photochem. Photobiol., B* **1996**, *33*, 171−180.
(46) Kay, A.; Humphry-Baker, R.; Graetzel, M. Artificial Photosynthesis. 2. Investigations on the Mechanism of Photosensitization of Nanocrystalline TiO2 Solar Cells by Chlorophyll Derivatives. *J. Phys. Chem.* **1994**, *98*, 952−959.
(47) Ferguson, G. S.; Chaudhury, M. K.; Sigal, G. B.; Whitesides, G. M. Contact Adhesion of Thin Gold Films on Elastomeric Supports: Cold Welding under Ambient Conditions. *Science (Washington, DC, U. S.)* **1991**, *253*, 776−778.
(48) Kéna-Cohen, S.; Davanço, M.; Forrest, S. R. Strong Exciton-Photon Coupling in an Organic Single Crystal Microcavity. *Phys. Rev. Lett.* **2008**, *101*, 116401.
(49) Würth, C.; Grabolle, M.; Pauli, J.; Spieles, M.; Resch-genger, U. Relative and Absolute Determination of Fluorescence Quantum Yields of Transparent Samples. *Nat. Protoc.* **2013**, *8*, 1535−1550.

DOI: 10.1021/acsphotonics.7b00679
ACS Photonics XXXX, XXX, XXX−XXX